Available online at www.sciencedirect.com
SCIENCE DIRECT
Journal of Sound and Vibration 295 (2006) 553–570
JOURNAL OF SOUND AND VIBRATION
www.elsevier.com/locate/jsvi

Transient growth and rotor–stator interaction noise in mean swirling duct flow

A.J. Cooper[a,*], N. Peake[b]

[a]School of Engineering, University of Warwick, Gibbet Hill Road, Coventry, CV4 7AL, UK
[b]Department of Applied Mathematics and Theoretical Physics, Centre for Mathematical Sciences, University of Cambridge, Wilberforce Road, Cambridge, CB3 0WA, UK

Received 5 October 2004; received in revised form 25 October 2005; accepted 4 January 2006
Available online 11 April 2006

Abstract

The phenomenon of spatial transient growth in swirling duct flow with application to aeroengine duct acoustics is investigated. In a typical aeroengine a region of swirling flow exists between the rotor and the downstream stator. The possibility for optimal transient growth of disturbance energy, and of a norm related to the acoustic power radiated back upstream from the stator is shown. Significant transient growth of both energy and noise norms can be observed over length scales relevant to aeroengine size, and over a wide range of parameter values such as the degree of mean swirl, azimuthal wavenumber and frequency. The optimal disturbances are found to have significant three dimensionality. The growth in energy results from increases in the azimuthal and radial components of the disturbance velocity field as it propagates downstream, whilst increases in the azimuthal velocity bring about non-modal growth of the noise measure.

1. Introduction

The phenomenon of aeroacoustic and fluid-dynamical instability and noise generation in aeroengines has traditionally been studied by considering the behaviour of infinitesimal unsteady disturbances. Generally these disturbances are assumed to be periodic, and are expressed as a modal decomposition so that the characteristic behaviour can be determined from the solution of an eigenvalue problem. This solution essentially describes the asymptotic, long-term or long-range, behaviour of the flow. In aeroengine intake ducts, where the mean flow is generally axial and irrotational, the eigenvalue problem derived from the governing acoustic wave equation leads to the identification of acoustic modes which describe the evolution of sound waves along the duct. Important stability and noise generation problems also occur, or are associated with, the region of *swirling* flow which occurs downstream of the rotor. The length of this swirl region is physically curtailed by the presence of a stator located further downstream. In the case of swirling flow the fluid motion is governed by acoustic and vorticity equations which are coupled by the presence of non-zero mean vorticity.

An important feature of swirling duct flow is that the underlying linear operator of the governing eigenvalue problem is non-normal and the associated eigenfunctions are non-orthogonal. In the field of stability theory

*Corresponding author. Fax: +2476 418922.
E-mail addresses: A.J.Cooper@warwick.ac.uk (A.J. Cooper), N.Peake@damtp.cam.ac.uk (N. Peake).

0022-460X/$ - see front matter © 2006 Elsevier Ltd. All rights reserved.
doi:10.1016/j.jsv.2006.01.051

Nomenclature

a_0	mean sound speed
$\mathbf{A}$	matrix, Eq. (19)
$\mathbf{B}$	matrix, Eq. (27)
$\mathbf{D}$	matrix, after Eq. (17)
G_E	maximum energy norm, Eq. (17)
G_N	maximum noise norm, Eq. (25)
$k_{1,2}$	Eq. (38)
$\mathbf{K}$	matrix, Eq. (12)
$\mathbf{L}$	matrix, Eq. (12)
m	azimuthal order
$\mathbf{M}$	matrix, Eq. (14)
$\mathbf{q}$	perturbation vector (before Eq. (13)),
$\mathbf{Q}$	matrix, Eq. (23)
$r_{h,t}$	hub and tip radii
$\mathbf{u}'$	velocity perturbation
$u_\perp$	blade normal velocity
U, W	axial, azimuthal mean flow speed
t	time
X, R, T	amplitudes of components of rotational unsteady velocity
x, r, θ	cylindrical polar coordinates
$Z_{1,2}$	inner, outer wall impedances
γ_ε	Eq. (29)
$\boldsymbol{\kappa}$	eigenvector, Eq. (20)
κ	after Eq. (37)
Φ	potential for irrotational part of unsteady flow
ϕ	amplitude of Φ
Λ	convective wavenumber—following Eq. (10)
ρ_0	mean density
σ	hub-to-tip ratio
$\boldsymbol{\xi}$	mean vorticity
Ω	solid-body swirl angular velocity
ω	frequency

and transition there has been great interest in the phenomenon of non-modal (algebraic) growth, whereby small disturbances may undergo significant transient growth before settling into the asymptotic state predicted by the modal eigenvalue analysis. Mathematically non-modal growth occurs as a result of the non-normality of the linearized operators describing the disturbance behaviour, and constructive and destructive interference is possible before modal behaviour sets in. Apparently this phenomenon has not been addressed previously in the context of duct acoustics.

A modal decomposition in swirling duct flow leads to the identification of two families of coupled acoustic-vorticity modes. One set is pressure-dominated, analogous to acoustic modes in non-swirling (irrotational) flow and maintained by compressibility effects. The other set is vorticity dominated and maintained by mean vorticity effects. The propagation of sound and vorticity waves can be expressed in terms of a superposition of these modes. Various aspects of swirling duct flow and the phenomena associated with it in aeroengine applications have been studied by a number of investigators. For example Roger and Arbey [1], Golubev and Atassi [2] and Tam and Auriault [3] considered the propagation of disturbances and identified the different families of eigenmodes. The role of swirl in the generation of acoustic resonance within aeroengine ducts, which may be relevant to the destabilization of the fan and the onset of flutter and rotating stall, has been considered by Cooper and Peake [4] and Cooper et al. [5]. More recently the effect of swirl on the generation of rotor–stator interaction noise has been investigated by Golubev and Atassi [6,7], Atassi et al. [8] and Cooper and Peake [9,10].

Numerous investigations into viscous flow problems have shown significant non-modal growth, both in temporal and spatial frameworks, even when all the eigenmodes are stable. Hultgren and Gustavsson [11] considered the temporal evolution of a 3-D disturbance in a boundary layer and found periods of initial algebraic growth followed by viscous decay. Other work using the temporal formulation to investigate the transient amplification of disturbances has been carried out by Boberg and Brosa [12], Butler and Farrell [14], Gustavsson [15], Reddy and Henningson [16], Schmid and Henningson [17] and Trefethen et al. [18], and all showed the possibility of significant non-modal growth effects. Work in the spatial framework followed [19–23]. Compressible flows studied in the temporal framework have been viscous compressible shear flow [24] and compressible boundary-layer flow [25] which showed a large amount of transient growth (temporal) over a wide range of parameter values. Tumin and Reshotko [23] considered transient growth effects in compressible boundary-layer flow in the spatial framework. The mechanism of optimal stationary disturbances in viscous rotating pipe flow and optimal temporal disturbances in a trailing vortex has been

explored recently by Ben-Dov et al. [26]. As a result of all these investigations the phenomenon of transient, non-modal, growth has been strongly associated with the so-called bypass transition and a possible mechanism that triggers nonlinear effects.

Since the linear operator for swirling duct flow is non-normal the question is posed as to whether non-modal effects may be significant in aeroengine acoustics applications. The effects of any non-modal growth would not be interpreted as a route to transition as in the studies in stability theory described above. Rather, it needs to be established whether any energy growth would have implications for rotor–stator interaction noise, or for the sort of resonant phenomenon described in Cooper and Peake [4]. Another difference to the stability theory studies lies with the fact that the region over which transient effects can occur is finite, so that if transient effects are present the length scale over which they occur in mean swirling duct flow must be compatible with the engine size to be physically relevant.

The purpose of this paper is therefore to investigate non-modal effects within a spatial framework, and to consider the growth of disturbance energy and of a so-called 'noise norm', which is related to the generation of rotor–stator interaction noise. A parametric study is undertaken to establish characteristic behaviour in terms of the degree of swirl, azimuthal mode number and frequency.

The mathematical background to the problem is described in Section 2, which introduces the governing equations and the inner products relevant to the optimal growth of disturbance energy and noise. Results are presented in Section 3, followed by a summary and conclusions in Section 4.

2. Mathematical background

2.1. Governing equations

The region downstream of the rotor in a typical aeroengine is modelled as an axisymmetric duct with circular cross-section described in terms of a cylindrical coordinate system (x, r, θ) where the x-axis points downstream. Lengths are non-dimensionalized by the tip radius, so that the duct is defined by the hub-tip ratio $\sigma = r_h/r_t$ and the flow region is $\sigma \leqslant r \leqslant 1$. Velocities are non-dimensionalized with respect to the stagnation speed of sound a_0^*, and subsequently all quantities used are non-dimensional.

The duct is assumed to carry a steady, swirling mean flow velocity, $\mathbf{U}(r)$, and a small-amplitude 3-D unsteady perturbation velocity, $\mathbf{u}'(x, r, \theta, t)$. The steady mean flow takes the form

$$\mathbf{U}(r) = U(r)\mathbf{e}_x + W(r)\mathbf{e}_\theta, \tag{1}$$

so that the mean vorticity, $\boldsymbol{\xi}$, is given by

$$\boldsymbol{\xi} = \frac{1}{r}\frac{\partial(rW)}{\partial r}\mathbf{e}_x - \frac{\partial U}{\partial r}\mathbf{e}_\theta. \tag{2}$$

The unsteady perturbation velocity is decomposed into vortical and potential parts according to Goldstein [27] so that the unsteady velocity and pressure are expressed as

$$\mathbf{u}' = \mathbf{u} + \boldsymbol{\nabla}\Phi, \quad p' = -\rho_0 \frac{D\Phi}{Dt}, \tag{3}$$

where $\rho_0(r)$ is the mean density and $D/Dt \equiv \partial/\partial t + \mathbf{U}\cdot\boldsymbol{\nabla}$ is the convective derivative.

The evolution of the unsteady disturbances is governed by the linearized Euler and continuity equations. Under the assumption of uniform mean entropy these equations can be written in the form

$$\frac{D\mathbf{u}}{Dt} + (\mathbf{u}\cdot\boldsymbol{\nabla})\mathbf{U} = -\boldsymbol{\xi}\times\boldsymbol{\nabla}\Phi, \tag{4}$$

$$\frac{D}{Dt}\frac{1}{a_0^2}\frac{D}{Dt}\Phi - \frac{1}{\rho_0}\boldsymbol{\nabla}\cdot(\rho_0\boldsymbol{\nabla})\Phi = \frac{1}{\rho_0}\boldsymbol{\nabla}\cdot(\rho_0\mathbf{u}), \tag{5}$$

where $a_0(r)$ is the local speed of sound. As can be seen the Euler (vorticity) and continuity (potential) equations are coupled by the presence of non-zero mean vorticity on the right-hand side of Eq. (4). In the absence of

mean vorticity $\mathbf{u}$ is decoupled from Φ, and can be determined explicitly in terms of the unsteady vortical flow at upstream infinity.

Assuming a disturbance of the form

$$(\Phi, \mathbf{u})(x, r, \theta, t) = (\Phi, u, v, w)(x, r, \theta, t) = (\phi, X, R, T)(r) \exp(\mathrm{i}\omega t - \mathrm{i}m\theta - \mathrm{i}kx), \tag{6}$$

where ω is the frequency, m is the azimuthal wavenumber, k is the axial wavenumber and (ϕ, X, R, T) denote the amplitudes of the corresponding unsteady quantities, the governing Eqs. (4) and (5) become

$$\mathrm{i}\Lambda X + \frac{\partial U}{\partial r}\left(\frac{\partial \phi}{\partial r} + R\right) = 0, \tag{7}$$

$$\mathrm{i}\Lambda R - \frac{2WT}{r} + \mathrm{i}k\frac{\partial U}{\partial r}\phi + \frac{\mathrm{i}m}{r}\frac{1}{r}\frac{\partial (rW)}{\partial r}\phi = 0, \tag{8}$$

$$\mathrm{i}\Lambda T + \frac{1}{r}\frac{\partial (rW)}{\partial r}\left(\frac{\partial \phi}{\partial r} + R\right) = 0, \tag{9}$$

$$\frac{\partial^2 \phi}{\partial r^2} + \left(\frac{1}{r} + \frac{\partial \ln \rho_0}{\partial r}\right)\frac{\partial \phi}{\partial r} + \left(\frac{\Lambda^2}{a_0^2} - \frac{m^2}{r^2} - k^2\right)\phi + \frac{\partial R}{\partial r} + \left(\frac{1}{r} + \frac{\partial \ln \rho_0}{\partial r}\right)R - \frac{\mathrm{i}mT}{r} - \mathrm{i}kX = 0, \tag{10}$$

where $\Lambda = \omega - kU - mW/r$. The case $\Lambda = 0$ corresponds to a disturbance which is exactly convected with the mean axial and swirling flows. The boundary conditions for a hard-walled duct require that the radial velocity vanishes at the duct walls, so that

$$\frac{\partial \phi}{\partial r} + R = 0 \quad \text{at } r = \sigma, 1. \tag{11}$$

Since the aim is to investigate *spatial* transient growth, the frequency and azimuthal wavenumber are fixed and the equations can be cast in the form of a linear axial eigenvalue problem

$$\mathbf{L}\boldsymbol{\psi} = k\mathbf{K}\boldsymbol{\psi}, \tag{12}$$

where $\boldsymbol{\psi} = (\phi, \eta, R, \mathrm{i}T)$ with $\eta = k(1 - U^2/a_0^2)\phi$. Eq. (12) is found by first eliminating X in Eq. (10) using Eq. (7), and then forming Eqs. (8–10) into the matrix equation. When Eq. (12) has been solved, the quantity X can be recovered from Eq. (7). The matrices $\mathbf{L}$ and $\mathbf{K}$ are given in the appendix. For aeroengine applications, where the mean vorticity is non-zero, the linear operator $\mathbf{L} - k\mathbf{K}$ is non-normal.

Since the governing equations are coupled acoustic-vorticity equations, solutions to the eigenvalue problem are coupled acoustic-vorticity waves and it is now well-known in the literature that two distinct families of eigenmodes are supported (see e.g. Refs. [2,3]). One set of eigenmodes propagates with phase speeds close to the speed of sound and are analogous to sound waves in a uniform flow. The second set of eigenmodes is nearly convected with the mean flow, is vorticity dominated and sustained by the mean vorticity. The first set is often referred to as 'pressure-dominated' in the literature, but it should be noted that the second set, having a phase speed which is not exactly convected, also possess a non-zero (but typically smaller) pressure themselves. The second set of eigenmodes all propagate downstream. Details on how the eigenmodes are determined numerically are given in the appendix. Typical eigenvalue spectra are shown in Fig. 1 for the case of uniform axial flow ($U = 0.3$) and rigid-body swirl ($W = 0.4r$) when $\sigma = 0.5$, $\omega = 15$ and $m = \pm 16$. The vorticity-dominated modes consist of two branches which asymptotically approach a singular point corresponding to pure convection (given by $\Lambda = 0$). These modes will subsequently be referred to as left and right rotational modes. The pressure-dominated modes generally consist of a finite number of propagating modes (real eigenvalues) referred to as cut-on modes, and an infinite set of evanescent modes (complex eigenvalues) referred to as cut-off modes. Cut-on modes which lie to the left/right of the cut-off modes propagate upstream/downstream. Note that there are no cut-on modes in this example when $m = 16$ and one upstream and one downstream cut-on mode when $m = -16$. This demonstrates a general trend with azimuthal wavenumber, described in detail by Roger and Arbey [1], in that modes co-rotating with the swirl ($m > 0$) can be cut-off by the mean swirl, but modes counter-rotating with the swirl ($m < 0$) can be cut-on by mean swirl.

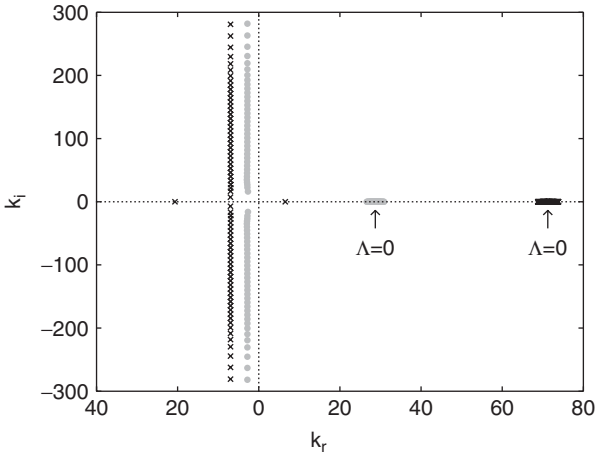

Fig. 1. Spatial eigenvalue spectrum for $U = 0.3$, $W = 0.4r$, $\omega = 15$, $\sigma = 0.5$. Grey circles: $m = 16$, crosses: $m = -16$.

2.2. Energy norm and optimal energy growth

In order to describe non-modal effects and the optimal growth of disturbance energy it is necessary to introduce an appropriate inner product and associated norm. Since the problem being considered is the spatial evolution of disturbances in a compressible flow a similar approach to Hanifi et al. [25] is used to define the inner product, which must involve both disturbance velocity and density. Given that $\mathbf{q} = (u', v', w', \rho')^{\mathrm{T}}$ then, for disturbance vectors $\mathbf{q}_j$ and $\mathbf{q}_k$, the scalar product based on energy density is

$$(\mathbf{q}_j, \mathbf{q}_k)_E = 2\pi \int_\sigma^1 \mathbf{q}_j^{\mathrm{H}} \mathbf{M} \mathbf{q}_k r \, \mathrm{d}r, \tag{13}$$

where H denotes complex conjugate transpose and

$$\mathbf{M} = \mathrm{diag}(\rho_0, \rho_0, \rho_0, a_0^2/\rho_0). \tag{14}$$

The associated energy norm is then

$$(\mathbf{q}, \mathbf{q})_E = \|\mathbf{q}\|_E^2. \tag{15}$$

Note that in the state vector $\mathbf{q}$ the velocity components u', v', w' are the components of the total perturbation velocity given by $\mathbf{u} + \nabla\Phi$ and the perturbation density is given by $\rho' = p'/a_0^2$. It should be noted that the choice of inner product determines both the qualitative and quantitative behaviour of the system; the energy norm yields that $\|\mathbf{q}\|_E^2$ is the quadratic energy density of the disturbance (i.e. kinetic plus potential), but other norms yield different measures of the disturbance amplitude. An energy equation for the flow could be written down, as in Goldstein [13], but it should be noted that $\|\mathbf{q}\|_E^2$ is not a conserved quantity due to the presence of the mean vortical flow.

The optimal transient growth is based on an eigenvalue expansion and is similar to the method first used by Butler and Farrell [14]. The optimal spatial energy growth is determined as an initial-value problem using the method developed for the temporal framework by Schmid and Henningson [17] and adapted by Reshotko and Tumin [22] for the spatial framework. The state vector is expanded in terms of the first M downstream eigenmodes, which either propagate or decay downstream, so that

$$\mathbf{q}(x, r, \theta, t) = \mathrm{e}^{\mathrm{i}\omega t - \mathrm{i}m\theta} \sum_{j=1}^{M} \kappa_j \hat{\mathbf{q}}_j(r) \mathrm{e}^{-\mathrm{i}k_j x}, \tag{16}$$

where $\hat{\mathbf{q}}_j$ is the jth eigenfunction corresponding to the jth eigenvalue k_j, and κ_j are coefficients to be optimized to give maximum energy growth. Since the downstream eigenvalue spectrum essentially consists of three branches of eigenmodes (left and right branches of the rotational modes and the cut-on/cut-off downstream

acoustic modes) the eigenmodes included in the expansion are chosen equally from each of these families. In ordering the eigenmodes the left and right branches of the rotational modes are counted starting furthest from the point of pure convection $\Lambda = 0$. For the acoustic modes the cut-on modes are counted first followed by the cut-off modes in order of increasing $|k_i|$. The M eigenmodes for the expansion then comprise the first N eigenmodes of each type, so that $M = 3N$.

The maximum energy growth at a specific downstream location is given by

$$G_E(\omega, m, x) = \max \frac{\|\mathbf{q}(x)\|_E^2}{\|\mathbf{q}(0)\|_E^2}, \tag{17}$$

where $\|\mathbf{q}(0)\|_E^2$ is the energy at the initial location $x = 0$, and the maximization is taken over all possible initial conditions $\mathbf{q}(0)$. Using the notation $\boldsymbol{\kappa} = (\kappa_1, \kappa_2, \ldots, \kappa_M)^{\mathrm{T}}$ and $\mathbf{D}$ for the matrix with $\exp(-\mathrm{i}k_j x)$ on the diagonal, the ratio of norms on the right-hand side of Eq. (17) can be rewritten in the form

$$\frac{\|\mathbf{q}(x)\|_E^2}{\|\mathbf{q}(0)\|_E^2} = \frac{\boldsymbol{\kappa}^{\mathrm{H}}\mathbf{D}^{\mathrm{H}}\mathbf{A}\,\mathbf{D}\boldsymbol{\kappa}}{\boldsymbol{\kappa}^{\mathrm{H}}\mathbf{A}\boldsymbol{\kappa}}, \tag{18}$$

where $\mathbf{A}$ is the matrix of inner products defined by

$$A_{jk} = (\mathbf{q}_j, \mathbf{q}_k)_E. \tag{19}$$

The maximum energy growth at a particular downstream location is then given by the largest eigenvalue of the problem

$$\mathbf{A}^{-1}\mathbf{D}^{\mathrm{H}}\mathbf{A}\,\mathbf{D}\,\boldsymbol{\kappa} = G_E(x)\boldsymbol{\kappa}, \tag{20}$$

where $G_E(x)$ is the eigenvalue. The corresponding eigenvector $\boldsymbol{\kappa}$ determines the expansion coefficients in Eq. (16) for the energy to be maximized at that axial location.

Recall here that we are considering the rotor–stator flow to be an axisymmetric mean base state plus an unsteady, non-axisymmetric perturbation. The rotor wakes themselves are therefore part of this perturbation. Note that the optimal energy growth G_E (and the optimal noise growth G_N defined below) are maximized over all possible initial conditions of disturbances launched from the trailing edges of the rotor. Traditionally, rotor wakes have been modelled using families of profiles (perhaps Gaussians), with adjustable parameters to account for wake width and depth varying along the blade span. It therefore follows that simple wake models, such as the Gaussian profiles, and indeed more realistic and complicated turbulent wake flows that one might obtain from an experiment or a large CFD calculation, are included within the space over which we optimize, and therefore that the optimal growth results we report provide an upper bound on what will occur in reality.

2.3. Noise norm

The emphasis is now changed from the non-modal growth of disturbance energy to consider an alternative measure of disturbance amplitude which may be more relevant to the noise levels generated when the downstream-propagating disturbances interact with the stator. The aim is to establish whether transient growth may have a significant impact on rotor–stator interaction noise.

One approach to this problem would involve considering a full linear system, in which the downstream disturbance at $x = 0$ is converted into an acoustic field upstream (or downstream) of the stator. However, in order to complete the optimal disturbance analysis complete information about the interaction, including the scattering of any given incoming mode into any given outgoing acoustic mode, would be needed. This could be completed in principle, but would require an exceedingly intensive computation of interactions with the stator. For present purposes a property of the incident disturbance alone is sought, which is closely related to the noise. The behaviour of this property can then be taken as being indicative of the possible effects of transient growth on noise generation.

Rotor–stator interaction noise results when the downstream unsteady field interacts with the stator blades. Several noise generation mechanisms arise here, including for instance volume terms associated with unsteady motion round the stator blades, but the dominant mechanism corresponds to the simple momentum-blocking effect when the unsteady flow is prevented from passing through the rigid stator blades. The amount of

momentum blocking depends crucially on the unsteady velocity normal to the blades, and for the typical high frequencies in these problems it can be shown [28] that the noise generated is proportional to the disturbance velocity normal to the stator blade at the blade leading edge. For an unloaded row of stator blades, assumed to be of zero thickness, aligned with the upstream steady flow, the blades make an angle α, defined by $\tan\alpha = W(r)/U(r)$, to the axis. The component of the incident unsteady velocity field normal to the stator blades is then given by

$$u_\perp = w' \cos\alpha - u' \sin\alpha. \tag{21}$$

A norm which is more indicative of the acoustic power radiated than the energy norm can then be formed by maximizing $u_\perp$ across the span of the duct. A scalar product appropriate for maximizing this is thus defined by

$$(\mathbf{q}_j, \mathbf{q}_k)_N = 2\pi \int_\sigma^1 \mathbf{q}_j^{\mathrm{H}} \mathbf{Q} \mathbf{q}_k r \, \mathrm{d}r, \tag{22}$$

where

$$\mathbf{Q} = \mathrm{diag}(-\sin\alpha, 0, \cos\alpha, 0), \tag{23}$$

and what is termed the associated 'noise norm' is

$$(\mathbf{q}, \mathbf{q})_N = \|\mathbf{q}\|_N^2. \tag{24}$$

The same eigenvalue expansion approach as used in the optimization of disturbance energy can be applied to optimize the noise norm. The noise norm is extremized relative to the same initial constraints as the disturbance energy by defining the maximum noise growth downstream as

$$G_N(\omega, m, x) = \max \frac{\|\mathbf{q}(x)\|_N^2}{\|\mathbf{q}(0)\|_E^2}. \tag{25}$$

The maximum noise norm is then determined as the largest eigenvalue of the problem

$$\mathbf{A}^{-1}\mathbf{D}^{\mathrm{H}}\mathbf{B}\mathbf{D}\boldsymbol{\kappa} = G_N(x)\boldsymbol{\kappa}, \tag{26}$$

where $\mathbf{A}$, $\mathbf{D}$ and $\boldsymbol{\kappa}$ are as defined in the previous section and

$$B_{jk} = (\mathbf{q}_j, \mathbf{q}_k)_N. \tag{27}$$

3. Results

The theory for optimal disturbances presented above is formulated for a general mean velocity distribution but there are some numerical difficulties in determining the rotational modes when Λ (defined after Eq. (10)) depends on the radius. Qualitative results can be obtained by approximating the mean velocity field by a uniform axial flow and solid-body rotation. Results are thus presented for the mean flow $U = U_0$, $W = \Omega r$, where U_0 and Ω are constants. This approximation allows more accurate and efficient computation of the eigenvalues and eigenvectors, which is crucial for optimal-growth considerations (we return to this point in the conclusions). For all the computations $N = 30$ eigenmodes of each type were included, which was found to be sufficient to give convergent solutions.

3.1. Energy norm

The first case examined considers the effect of the different families of eigenmodes on the maximum energy growth over the axial range $0 \leqslant x \leqslant 0.5$, when $\sigma = 0.5$, $U_0 = 0.3$ and $\omega = 15$. Fig. 2 shows the results for $m = 16$ and two different levels of mean swirl given by $\Omega = 0.1$ and 0.4 (both cases for which no cut-on modes occur). With only rotational modes included there is no transient growth and when only acoustic modes are included the energy decays with axial distance. In Fig. 2(c) the decay rate for $\Omega = 0.4$ is faster than that for $\Omega = 0.1$ since increasing the mean swirl produces modes which are more cut-off (larger values of $|k_i|$). With all modes included, however, transient growth effects are clearly visible indicating that acoustic–rotational

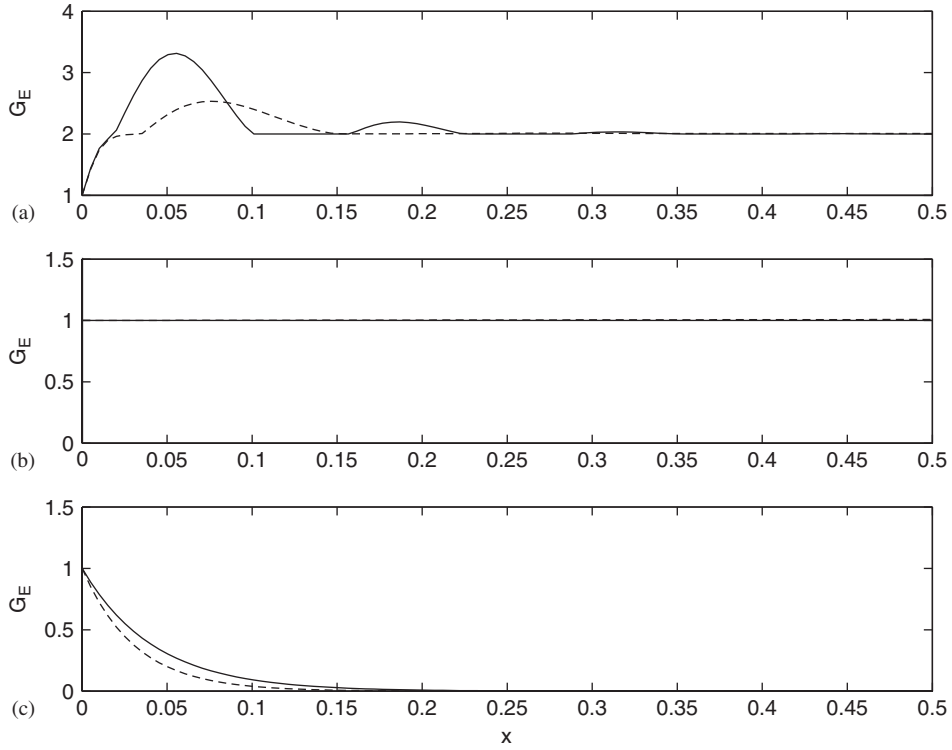

Fig. 2. Effect of different families of eigenmodes on maximum transient growth of energy (G_E) when $m = 16$, $\omega = 15$, $\sigma = 0.5$, $U_0 = 0.3$. Solid lines: $\Omega = 0.1$, dashed lines: $\Omega = 0.4$. (a) All eigenmodes included, (b) only rotational modes included, (c) only acoustic (cut-off) modes included.

interaction is vital for any transient growth effects to occur. The effect of swirl in this case is observed most over the axial range $0 \leqslant x \leqslant 0.25$ with lower levels of the mean swirl resulting in larger transient growth levels. This trend can be explained in terms of the effect of mean swirl on the cut-off modes. The amount of transient growth observed appears to be related to the rate of decay of the cut-off acoustic modes (the faster the decay the lower the maximum level of transient growth). This is further supported by the corresponding results when $m = -16$ which are shown in Fig. 3. In this case increasing the mean swirl tends to cut-on modes and a single mode is cut-on when $\Omega = 0.4$. As a result, the transient growth is higher for $\Omega = 0.4$ than for $\Omega = 0.1$ (since the cut-off acoustic modes decay less rapidly in the former case, while phase interference between the propagating acoustic mode and the nearly convected modes leads to oscillation in $G_E(x)$ for $\Omega = 0.4$). It must be emphasized that the transient growth is associated with the presence of mean vorticity—if $\Omega = 0$ then $G_E(x) \leqslant 1$ for all x.

It is also possible to identify which parts of the eigenvalue spectrum contribute most to the energy growth by considering the structure of the inner product matrix $\mathbf{A}$ defined in Eq. (19). This is shown in Fig. 4 when $m = 16$. The left branch of the rotational modes occupies the sites $j = 1$–30, the right branch sites $j = 31$–60 and the acoustic modes are in sites $j = 61$–90. The band of non-negligible inner products is widest for rotational–acoustic interactions (A_{jk} where $(j,k) = (61\text{–}90,1\text{–}60)$ and $(j,k) = (1\text{–}60,61\text{–}90)$) which supports the theory that both of these families of modes must be present for any non-modal growth to occur.

Another measure of transient growth effects can be obtained by considering the ε-pseudospectra. Normal operator behaviour can be represented by its eigenvalues spectrum, but for non-normal operators it is more appropriate to consider the pseudospectrum. The ε-pseudospectrum of the matrix $\mathbf{A}$ is defined in Schmid and Henningson [17] as

$$z \in \mathbb{C} \text{ such that } \|(z\mathbf{I} - \mathbf{A})^{-1}\|_E \geqslant \varepsilon^{-1}, \tag{28}$$

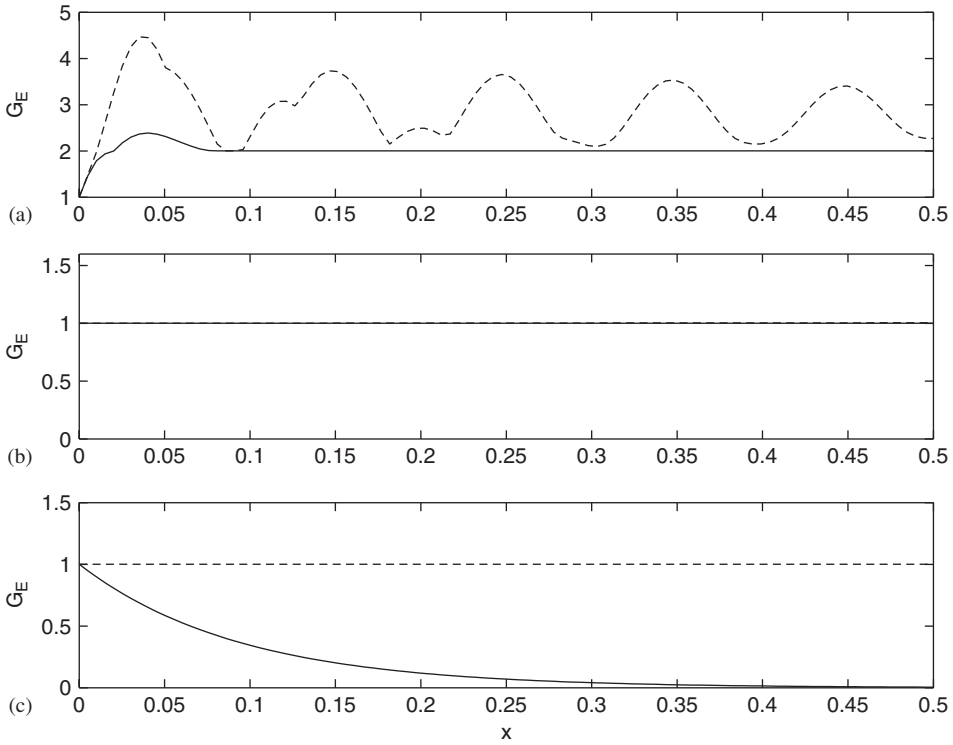

Fig. 3. Effect of different families of eigenmodes on maximum transient growth of energy (G_E) when $m = -16$, $\omega = 15$, $\sigma = 0.5$, $U_0 = 0.3$. Solid lines: $\Omega = 0.1$, dashed lines: $\Omega = 0.4$. (a) All eigenmodes included, (b) only rotational modes included, (c) only acoustic modes included (all cut-off when $\Omega = 0.1$ and one cut-on when $\Omega = 0.4$).

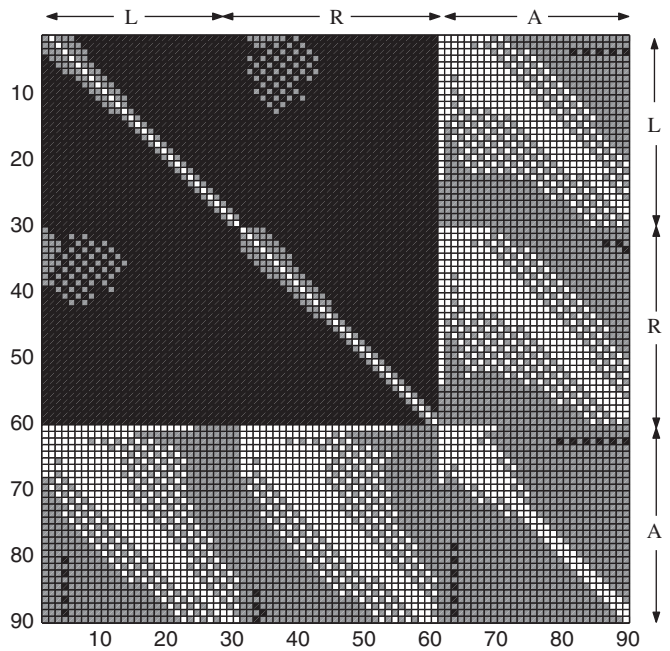

Fig. 4. Representation of inner product matrix **A** defined in Eq. (19) for $m = 16$, $U_0 = 0.3$, $\Omega = 0.4$, $\omega = 15$, $\sigma = 0.5$. Black regions are for $\ln|A_{jk}| < -14$, grey for $-14 \leqslant \ln|A_{jk}| < -10$ and white for $-10 \leqslant \ln|A_{jk}|$. Acoustic modes are labelled 'A', and left/right rotational modes by 'L/R'.

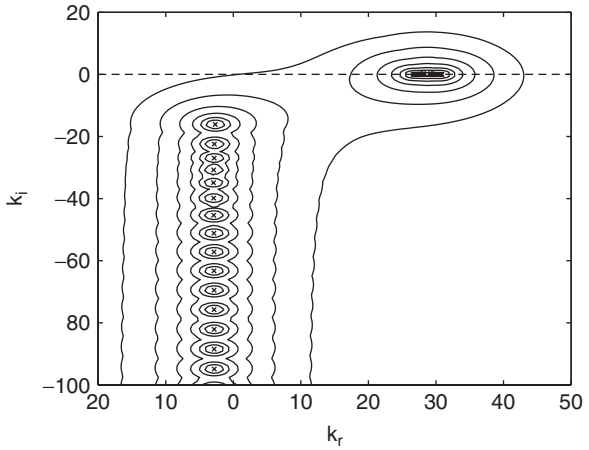

Fig. 5. ε-pseudospectrum for $m = 16$, $U_0 = 0.3$, $\Omega = 0.4$, $\omega = 15$, $\sigma = 0.5$. Crosses represent the downstream eigenvalue spectrum and the lines (from the outside inward) are the pseudospectral boundaries for $\varepsilon = 1, 10^{-0.2}, 10^{-0.4}, 10^{-0.6}, 10^{-0.8}, 10^{-1}$.

where **I** is the identity matrix. The pseudospectrum can be used to obtain a lower bound for the maximum of the expected transient growth. This is given by the Hille-Yosida Theorem [29,30] and is related to the extent to which the pseudospectrum protrudes into the unstable (upper) half-plane and is determined as

$$G_E \geqslant \gamma_\varepsilon^2 \quad \text{where } \gamma_\varepsilon \equiv \sup_{\varepsilon \geqslant 0} \frac{\beta(\varepsilon)}{\varepsilon}, \tag{29}$$

with $\beta(\varepsilon)$ the maximum imaginary part of the ε-pseudospectrum in the unstable (upper) half-plane. Fig. 5 shows the ε-pseudospectrum calculated for $m = 16$, $\Omega = 0.4$ which gives a lower estimate of $G_E = 1.96$ for the maximum energy growth which is consistent with the result in Fig. 2. The pseudospectrum is important because it provides an indication of the likely importance of the non-normal behaviour of the system—in effect the more the pseudospectra protrude into the upper half of the k-plane then the stronger the optimal growth will be.

The initial conditions which produce the optimal energy growth at specific axial locations are shown for $m = 16$ in Fig. 6 and for $m = -16$ in Fig. 7. In both cases the optimal disturbances have significant three-dimensionality and tend to be mostly tip-dominated, particularly in the density perturbation. As the optimal unsteady field evolves downstream the non-modal growth in disturbance energy occurs through increases in the radial (v') and azimuthal (w') velocity components, although the energy gains for $m = 16$ at the selected axial location are quite modest. The first few modal coefficients (κ_j) of each type of mode are found generally to be the largest, which means that the optimal disturbances possess significant pressure and vorticity.

The results of a parametric study across a range of azimuthal wavenumbers and frequencies are shown in Fig. 8. At the fixed frequency $\omega = 15$ and fixed flow conditions $U_0 = 0.3, \Omega = 0.4$, Fig. 8(a) shows significant transient growth effects can occur across a wide range of azimuthal wavenumbers. Fig. 8(b) plots the maximum of G_E over the axial range as a function of m and ω. Generally the level of growth increases with frequency and the largest growth (of almost a factor 6) occurs for negative values of m and when cut-on modes exist for positive values of m.

3.2. Noise norm

The effect of different levels of mean swirl on the results optimized for the noise norm are shown in Fig. 9. As with the optimal growth of disturbance energy increasing the mean swirl results in lower short-range growth at $m = 16$, compared to when $m = -16$. However, the growth obtained when $m = -16$ is now much lower than that when $m = 16$, a trend which is opposite to that observed for the energy growth. The initial conditions producing maximum growth of the noise norm at $x = 0.125$ when $m = 16$ and at $x = 0.25$ when

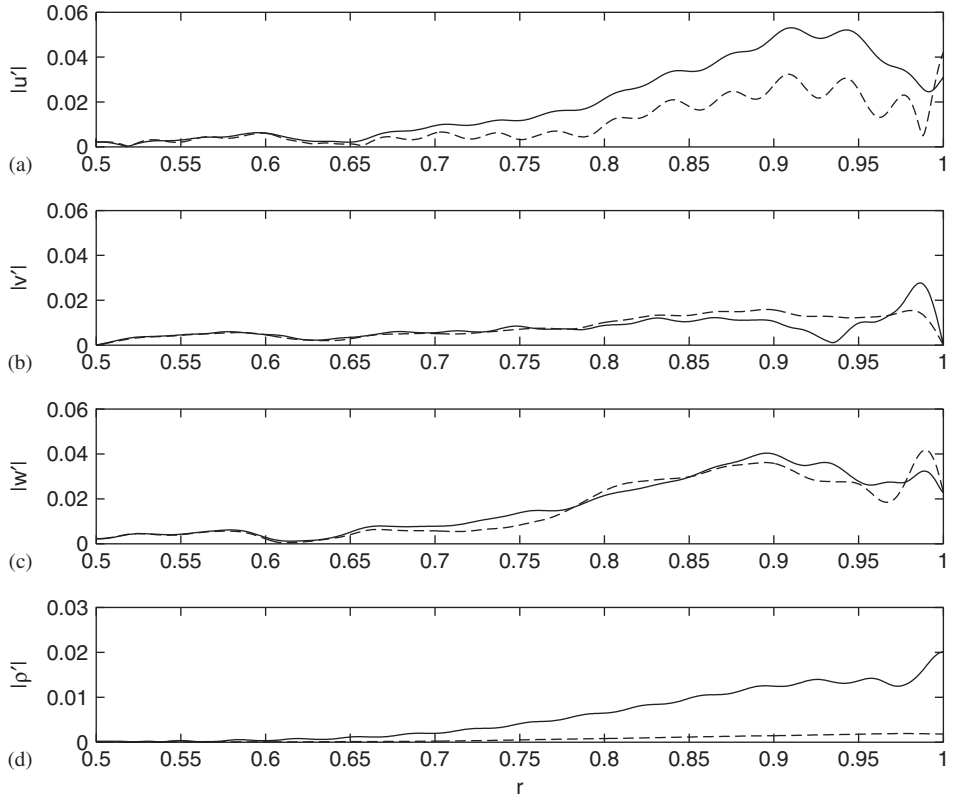

Fig. 6. Magnitude of components of state vector $\mathbf{q}$ for optimal energy growth at $x = 0.125$ when $m = 16$. Solid lines: initial conditions ($x = 0$), dashed lines: evolved profile at $x = 0.125$. (a) Axial disturbance velocity $|u'|$, (b) radial disturbance velocity $|v'|$, (c) azimuthal disturbance velocity $|w'|$, (d) disturbance density $|\rho'|$.

$m = -16$ are plotted in Fig. 10. As can be seen the velocity components take a very different form from those which produce optimal energy growth, with maximum velocity amplitude occurring at midspan when $m = 16$ and much more oscillatory profiles when $m = -16$. The largest modal coefficients are still the first few of each mode type when $m = 16$, but when $m = -16$ the largest coefficients are in the midrange of each mode type, which explains the more oscillatory form of the optimal initial disturbance. The growth of the noise norm is found generally to occur as a result of increases in the azimuthal velocity component. The optimal noise-norm growth is lower than that for the energy, owing largely to the contribution from the radial velocity in the energy norm being absent in the noise norm.

A parametric study across azimuthal wavenumber for the noise norm shows that the largest gains are confined to positive values of m and the growth in the noise norm (at fixed frequency) becomes less as m becomes more negative. Variation in the maximum of G_N with frequency shows similar trends to the energy growth, in that larger transient growth effects are observed as the frequency increases—see Fig. 11(a). Perhaps a more natural measure of the noise-norm growth is to consider the values at a fixed axial position representing the typical stator location in the duct. This is shown in Fig. 11(b) and indicates that there is an optimal azimuthal wavenumber m for which G_N is largest at the stator location. This value of m becomes larger as the frequency is increased.

3.3. Effect of lining

In practice sound can be attenuated in the duct through the application of acoustic lining on the duct walls. For an interstage lining with impedance $Z_{1,2}$ on the inner and outer walls respectively, the finite-impedance

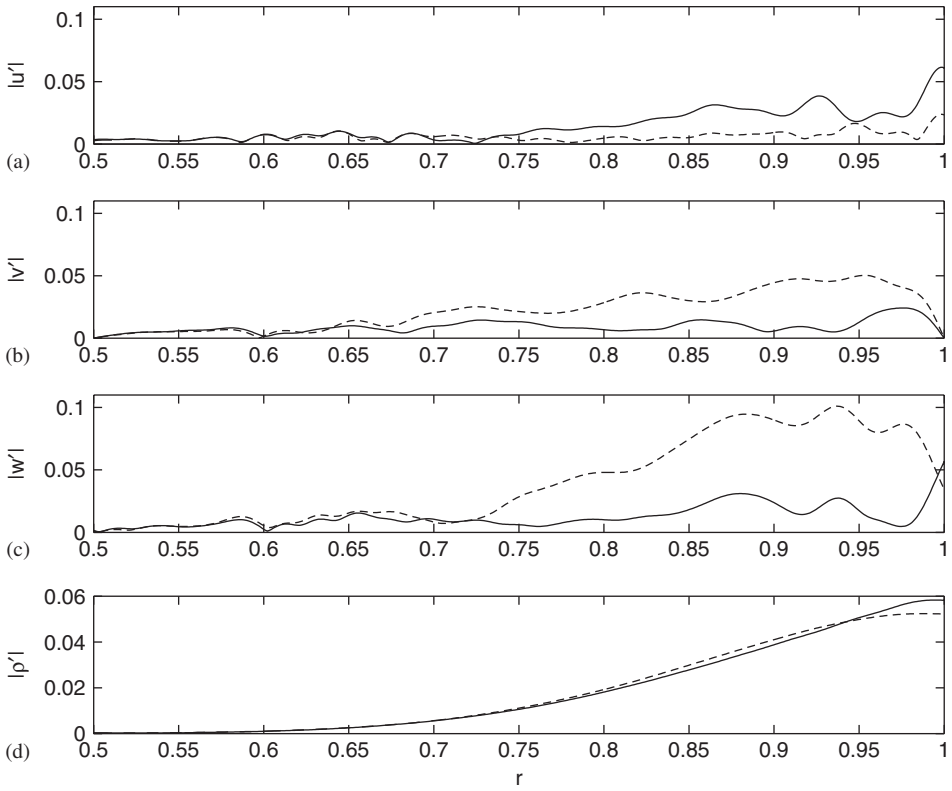

Fig. 7. Magnitude of components of state vector $\mathbf{q}$ for optimal energy growth at $x = 0.25$ when $m = -16$. Solid lines: initial conditions ($x = 0$), dashed lines: evolved profile at $x = 0.25$. (a) Axial disturbance velocity $|u'|$, (b) radial disturbance velocity $|v'|$, (c) azimuthal disturbance velocity $|w'|$, (d) disturbance density $|\rho'|$.

boundary conditions become

$$\mathrm{i}\omega\left(\frac{\partial\phi}{\partial r} + R\right) \pm \frac{\Lambda^2\rho_0\phi}{Z_{1,2}} = 0 \quad \text{at } r = \sigma, 1. \tag{30}$$

Hard-wall boundary conditions are recovered in the limit $Z_{1,2} \to \infty$.

This form of lining has the most effect on the acoustic modes, and attenuates modes which are cut-on in the hard-walled duct. There is no significant effect on the rotational modes, owing to the small pressure associated with these modes. Acoustic lining is found to be effective only for the attenuation of the energy growth when cut-on modes exist and when the outer wall is lined (since the cut-on eigenfunctions tend to be tip-dominated) and even then, as shown in Fig. 12, the lining has no effect on the maximum optimal growth attained but does reduce the optimal growth as x increases. There is little effect on the growth of the noise norm, since the cut-on modes do not contribute significantly to the optimal disturbance in this case. The effect of the liner on the transient growth is negligible when no cut-on modes exist in the hard-walled case, so that if any potentially damaging growth occurs then this cannot always be controlled by the use of a liner.

4. Summary and conclusions

Optimal disturbances in mean swirling duct flow can be identified whose spatial development leads to optimal non-modal growth in disturbance energy and in a measure aimed at optimizing upstream-radiated rotor–stator interaction noise. These optimal disturbances are constructed from eigenmodes which either propagate or decay downstream, and calculations show that interaction between the acoustic and rotational modes of swirling duct flow is essential for any transient growth to occur.

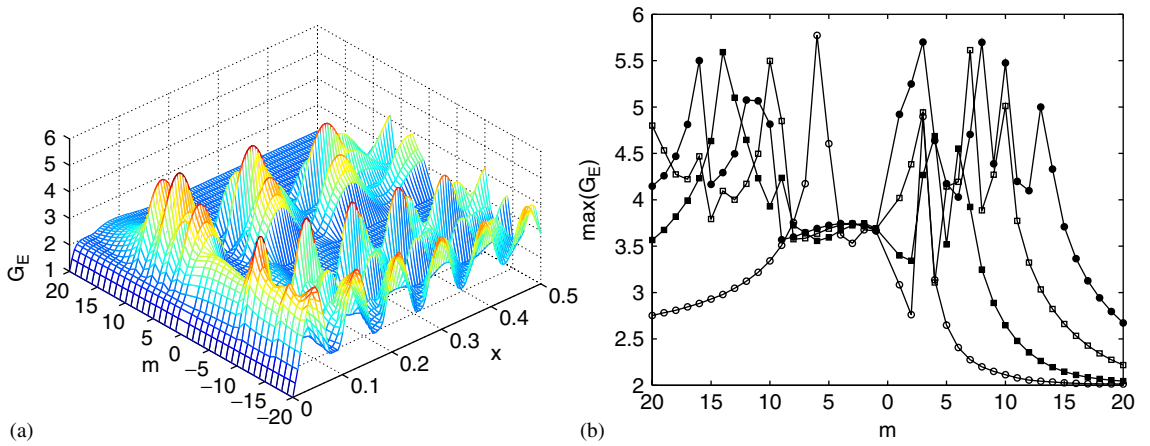

Fig. 8. (a) Variation of optimal growth of kinetic energy (G_E) with azimuthal wavenumber (m) and axial distance (x) when $\omega = 15$. (b) Variation of maximum optimal growth (maximized over x) with azimuthal wavenumber and frequency. Open circles: $\omega = 5$, filled squares: $\omega = 10$, open squares: $\omega = 15$, filled circles: $\omega = 20$. ($\sigma = 0.5$, $U_0 = 0.3$ and $\Omega = 0.4$.)

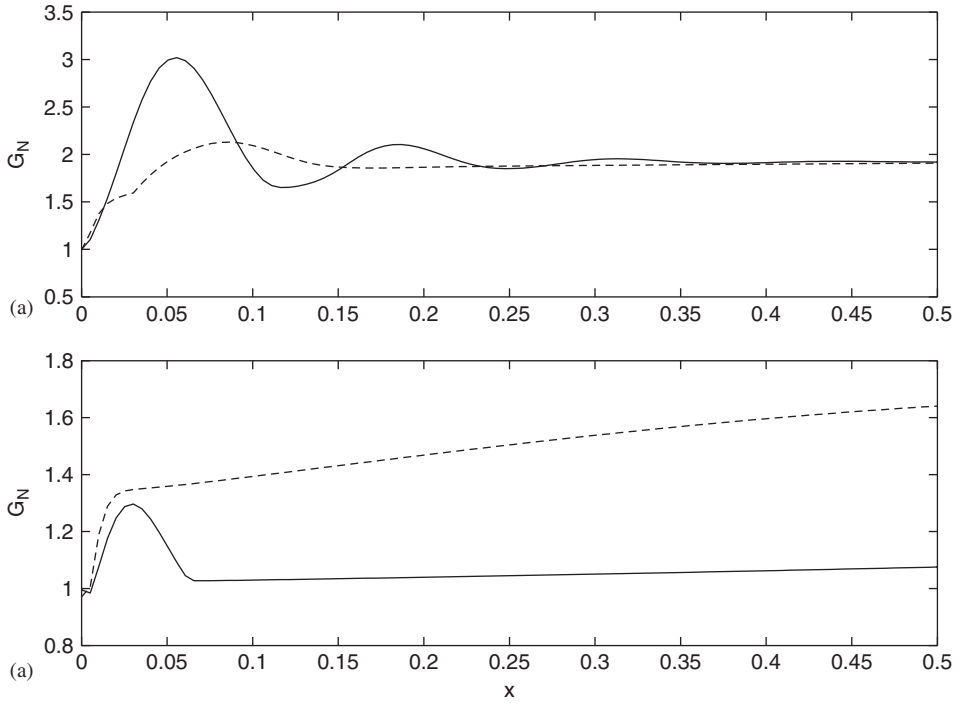

Fig. 9. Effect of swirl on maximum transient growth of noise norm (G_N) when $\omega = 15$, $\sigma = 0.5$, $U_0 = 0.3$. Solid lines: $\Omega = 0.1$, dashed lines: $\Omega = 0.4$. (a) $m = 16$, (b) $m = -16$.

For the mean flow consisting of uniform axial velocity and rigid-body swirl, energy gains of up to six fold can be sustained over distances which are physically relevant to aeroengine length scales. These energy gains will not trigger nonlinear effects in the way the non-normal effects may lead to transition in pipe flow, but may be large enough to impact on the acoustic resonance phenomenon described in Cooper and Peake [4] and Cooper et al. [5] and other aeroacoustic instabilities. Transient growth effects are also clearly visible in the noise norm, with up to a three-fold increase being observed for the flow conditions investigated (note that a three-fold increase corresponds to 4.8 dB on a PWL scale). Importantly, this form of non-modal growth cannot always be controlled with the use of acoustic wall lining. In the examples presented wall lining is only

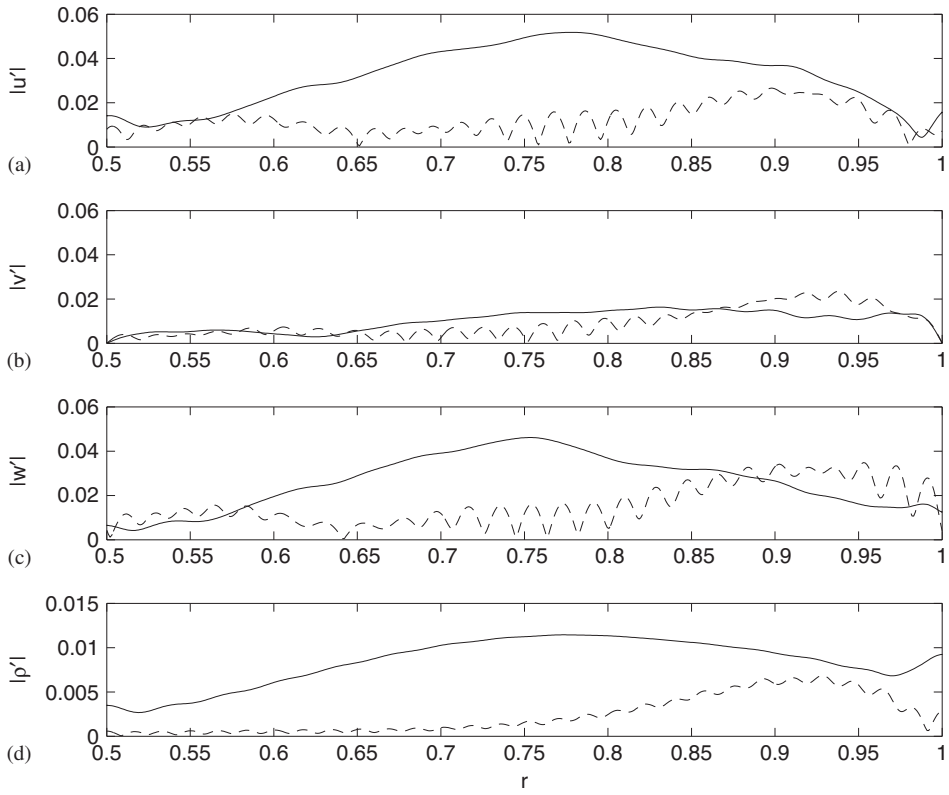

Fig. 10. Initial conditions which give maximum growth of the noise norm G_N at $x = 0.125$ when $m = 16$ (solid lines), and at $x = 0.25$ when $m = -16$ (dashed lines).

effective in attenuating some of the cut-on (propagating) acoustic modes, which do not necessarily contribute significantly to the transient growth.

The form of the optimal disturbances depends on the axial location at which optimal growth occurs and also depends on azimuthal wavenumber. The structure of the optimal disturbances varies between the two norms investigated but in all cases the optimal disturbances are 3-D. Growth in disturbance energy results from increases in azimuthal and radial disturbance velocity and growth in the noise norm results from increases in azimuthal disturbance velocity. In order for the transient growth effects to be physically relevant it would need to be established whether the disturbance profiles predicted by the optimal theory are physically realizable. However, it should be noted that turbulent rotor wakes and casing boundary layers will provide a broadband range of initial conditions, from which the optimal ones may be selected. Of course, if the optimal part of the forcing is present, but with very much lower amplitude than non-optimal parts, then one would be forced to say that the amplification due to non-normality may not be important. The point at which the non-normality becomes important is when the initial conditions actually do contain a significant projection onto the optimal initial condition. In that sense the present work is a first study, and further investigation is required into precisely how relevant these optimal initial conditions are, or put another way how close to our upper bounds a real system would come in practise.

Finally, we repeat that our calculations have been completed for the simplified case of solid-body swirl with uniform axial flow. This may be a reasonable approximation to the flow in a real aeroengine at mid-span, but is likely to be less representative close to the outer casing. Since the optimal initial conditions for the energy norm seen in Fig. 6 tend to be tip dominated, it is clear that further work is required in order to precisely quantify these effects for a real engine (in contrast, note that the optimal initial conditions for the noise norm seen in Fig. 10 tend to be mid-span dominated). The simplification provided by the solid-body swirl with uniform axial flow is that the wavenumber Λ is independent of r. For a general mean flow, $\Lambda = \Lambda(r)$, and the

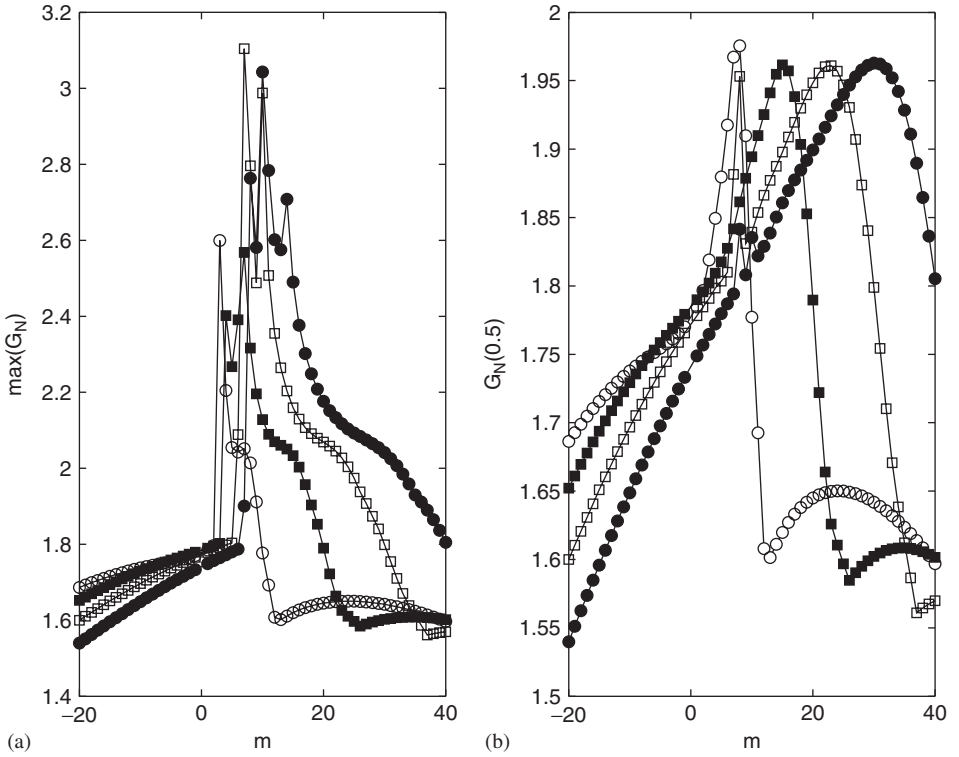

Fig. 11. (a) Maximum of $G_N(x)$ attained over $0 \leqslant x \leqslant 0.5$ as a function of azimuthal wavenumber, m, for frequencies $\omega = 5, 10, 15, 20$. (b) Variation of $G_N(x = 0.5)$ with m and ω. Open circles: $\omega = 5$, filled squares: $\omega = 10$, open squares: $\omega = 15$, filled circles: $\omega = 20$. ($\sigma = 0.5$, $U_0 = 0.3$ and $\Omega = 0.4$.)

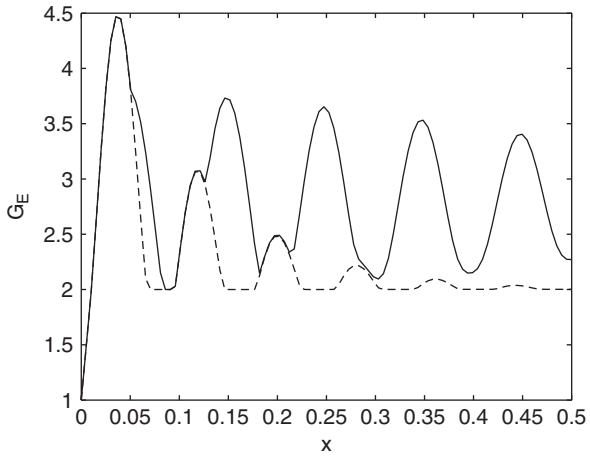

Fig. 12. Effect of acoustic lining on $G_E(x)$ when $m = -16$, $\omega = 15$, $U_0 = 0.3$, $\Omega = 0.4$ and $\sigma = 0.5$. Solid line: hard-walled duct; dashed line: lined outer wall ($Z_2 = 2 - i$).

problem possesses a non-trivial continuous spectrum. Recently, Heaton and Peake [32] have shown that this continuous spectrum can produce algebraic growth downstream, which is likely to lead to a significant enhancement of the growth of optimal disturbances. We therefore suggest that the results presented in this paper for solid-body swirl with uniform axial flow are likely to underestimate the transient growth possible in a real system, but this point needs a great deal of further investigation. We also note that the effects of

non-uniform mean entropy on the modal spectrum in swirling flow, excluded in this paper, have been investigated recently by Cooper [33], and that this is another effect which could well lead to enhanced non-normal behaviour.

Acknowledgements

The authors are very grateful to Dr. MCM Wright for suggesting the application of these techniques to this problem. AJC acknowledges funding from The Royal Society.

Appendix A. Numerical calculation of eigenvalues and eigenfunctions

Different numerical techniques are used to solve the eigenvalue problem (7)–(10) for the acoustic and rotational modes when the mean flow takes the form $U = U_0$, $W = \Omega r$, where U_0 and Ω are constants.

A.1. Acoustic modes

Initial estimates from the eigenvalues are obtained by solving the eigenvalue problem (12) using the global Chebyshev collocation technique described by Khorrami [31]. Since a large number of eigenmodes are required, the higher-order eigenfunctions are not always accurately resolved using this method. The eigenvalues and eigenfunctions are refined by using the values determined by the collocation technique as initial guesses in a local integration scheme. Under the assumptions of uniform axial flow and rigid-body rotation the vortical part of the unsteady velocity can be expressed in the form

$$X = 0, \tag{31}$$

$$R = \frac{1}{\Lambda^2 - 4\Omega^2}\left[\frac{-2\Omega m\Lambda\phi}{r} + 4\Omega^2\frac{\partial\phi}{\partial r}\right], \tag{32}$$

$$\mathrm{i}T = \frac{2\Omega}{\Lambda^2 - 4\Omega^2}\left[\frac{2\Omega m\phi}{r} - \Lambda\frac{\partial\phi}{\partial r}\right]. \tag{33}$$

A single equation for ϕ can then be derived

$$\frac{\partial^2\phi}{\partial r^2} + \left(\frac{1}{r} + \frac{\partial \ln\rho_0}{\partial r}\right)\frac{\partial\phi}{\partial r} + \left[\left(\frac{\Lambda^2 - 4\Omega^2}{\Lambda^2}\right)\left(\frac{\Lambda^2}{a_0^2} - k^2\right) - \frac{m^2}{r^2} - \frac{2\Omega m}{r\Lambda}\frac{\partial \ln\rho_0}{\partial r}\right]\phi = 0, \tag{34}$$

which, together with the boundary conditions

$$\frac{\partial\phi}{\partial r} - \frac{2\Omega m\phi}{r\Lambda} = 0 \quad \text{at } r = \sigma, 1, \tag{35}$$

is solved for ϕ using a fourth-order Runge–Kutta integration scheme. The functions R and T can then be determined from Eqs. (32) and (33). Eq. (34) is fully consistent with the equation solved by Roger and Arbey [1].

A.2. Rotational modes

Since these modes are sustained by swirl and not compressibility effects they can be determined by solving the reduced equation introduced by Tam and Auriault [3],

$$\frac{\partial^2\phi}{\partial r^2} + \frac{1}{r}\frac{\partial\phi}{\partial r} + \left[\frac{k^2(4\Omega^2 - \Lambda^2)}{\Lambda^2} - \frac{m^2}{r^2}\right]\phi = 0, \tag{36}$$

with boundary conditions as given in Eq. (35). The general solution to Eq. (36) is

$$\phi = J_m(\kappa r) + NY_m(\kappa r), \tag{37}$$

where J_m and Y_m are mth-order Bessel functions of the first and second kind respectively, N is an arbitrary constant and $\kappa = k(4\Omega^2 - \Lambda^2)^{1/2}/\Lambda$. The branch cuts of the square root in κ determine that propagating modes are possible in the range $k_1 < k < k_2$ where

$$k_1 = \frac{\omega - (2+m)\Omega}{U_0}, \quad k_2 = \frac{\omega + (2-m)\Omega}{U_0}. \tag{38}$$

Substitution into the boundary conditions and eliminating N gives the following dispersion relation for the eigenvalues k

$$\left[\kappa J'_m(\kappa\sigma) - \frac{2m\Omega}{\Lambda\sigma} J_m(\kappa\sigma)\right]\left[\kappa Y'_m(\kappa) - \frac{2m\Omega}{\Lambda} Y_m(\kappa)\right] - \left[\kappa J'_m(\kappa) - \frac{2m\Omega}{\Lambda} J_m(\kappa)\right]\left[\kappa Y'_m(\kappa\sigma) - \frac{2m\Omega}{\Lambda\sigma} Y_m(\kappa\sigma)\right] = 0. \tag{39}$$

Once the eigenvalues have been obtained the constant N can be determined. The solutions for R and T follow as for the acoustic modes.

Appendix B. Matrix operators

In Eq. (12), and in the specific case of solid-body swirl with uniform axial flow, the matrices are given by

$$\mathbf{L} = \begin{pmatrix} \mathbf{P} & -\dfrac{2(\omega - m\Omega)U_0\rho_0}{a_0^2\beta_0^2} & \rho_0\dfrac{\partial}{\partial r} + \dfrac{1}{r}\dfrac{\partial(r\rho_0)}{\partial r} & -\dfrac{m\rho_0}{r} \\ 0 & \dfrac{1}{\beta_0^2} & 0 & 0 \\ \dfrac{2m\Omega}{r} & 0 & \omega - m\Omega & 2\Omega \\ 2\Omega\dfrac{\partial}{\partial r} & 0 & 2\Omega & \omega - m\Omega \end{pmatrix}, \tag{40}$$

$$\mathbf{K} = \begin{pmatrix} 0 & \rho_0 & 0 & 0 \\ 1 & 0 & 0 & 0 \\ 0 & 0 & U_0 & 0 \\ 0 & 0 & 0 & U_0 \end{pmatrix}, \tag{41}$$

where

$$\mathbf{P} \equiv \frac{1}{r}\frac{\partial}{\partial r}\left(r\rho_0\frac{\partial}{\partial r}\right) + \rho_0\left(\frac{(\omega - m\Omega)^2}{a_0^2} - \frac{m^2}{r^2}\right). \tag{42}$$

and $\beta_0^2 \equiv 1 - U_0^2/a_0^2$.

References

[1] M. Roger, H. Arbey, Relation de dispersion des ondes de pression dans un écoulement tournant, *Acustica* 59 (1985) 95–101.

[2] V.V. Golubev, H.M. Atassi, Acoustic-vorticity waves in swirling flows, *Journal of Sound and Vibration* 209 (1998) 203–222.

[3] C.K.W. Tam, L. Auriault, The wave modes in ducted swirling flows, *Journal of Fluid Mechanics* 371 (1998) 1–20.

[4] A.J. Cooper, N. Peake, Trapped acoustic modes in aeroengine intakes with swirling flow, *Journal of Fluid Mechanics* 419 (2000) 151–173.

[5] A.J. Cooper, A.B. Parry, N. Peake, Acoustic resonance in aeroengine intake ducts, *ASME Journal of Turbomachinery* 126 (2004) 432–441.

[6] V.V. Golubev, H.M. Atassi, Unsteady swirling flows in annular cascade—part 1: evolution of incident disturbances, *AIAA Journal* 38 (2000) 1142–1149.

[7] V.V. Golubev, H.M. Atassi, Unsteady swirling flows in annular cascade—part 2: aerodynamic blade response, *AIAA Journal* 38 (2000) 1150–1158.
[8] H.M. Atassi, A.A. Ali, O.V. Atassi, I.V. Vinogradov, Scattering of incident disturbances by an annular cascade in swirling flow, *Journal of Fluid Mechanics* 499 (2004) 111–138.
[9] A.J. Cooper, N. Peake, Upstream-radiated rotor–stator interaction noise in mean swirling flow, *Journal of Fluid Mechanics* 523 (2005) 99–133.
[10] A.J. Cooper, N. Peake, Rotor–stator interaction noise in swirling flow: stator sweep and lean effects, *AIAA Journal* (2006), to appear.
[11] L.S. Hultgren, L.H. Gustavsson, Algebraic growth of disturbances in a laminar boundary layer, *Physics of Fluids* 24 (1981) 1000–1004.
[12] L. Boberg, U. Brosa, Onset of turbulence in a pipe, *Zeitschrift fur Naturforschung, Section A—Journal of Physical Sciences* 43 (1988) 697.
[13] M.E. Goldstein, *Aeroacoustics*, McGraw-Hill, New York, 1976.
[14] K.M. Butler, B.F. Farrell, Three-dimensional optimal perturbations in viscous shear flow, *Physics of Fluids* 4 (1992) 1637–1650.
[15] L.H. Gustavsson, Energy growth of three-dimensional disturbances in plane Poiseuille flow, *Journal of Fluid Mechanics* 224 (1991) 241–260.
[16] S.C. Reddy, D.S. Henningson, Energy growth in viscous channel flows, *Journal of Fluid Mechanics* 252 (1993) 209–238.
[17] P.J. Schmid, D.S. Henningson, Optimal energy density growth in Hagen–Poiseuille flow, *Journal of Fluid Mechanics* 277 (1994) 197–225.
[18] L.N. Trefethen, A.E. Trefethen, S.C. Reddy, T.A. Driscoll, Hydrodynamic stability without eigenvalues, *Science* 261 (1993) 578–584.
[19] P. Luchini, Reynolds number independent instability of the Blasius boundary-layer over a flat surface, *Journal of Fluid Mechanics* 327 (1996) 101–115.
[20] P. Luchini, Reynolds number independent instability of the boundary layer over a flat surface—part 2: optimal perturbations, *Journal of Fluid Mechanics* 404 (2000) 289–309.
[21] P. Andersson, M. Berggren, D.S. Henningson, Optimal disturbances and bypass transition in boundary layers, *Physics of Fluids* 11 (1999) 134–150.
[22] E. Reshotko, A. Tumin, Spatial theory of optimal disturbances in a circular pipe flow, *Physics of Fluids* 13 (2001) 991–996.
[23] A. Tumin, E. Reshotko, Spatial theory of optimal disturbances in boundary layers, *Physics of Fluids* 13 (2001) 2097–2104.
[24] B.F. Farrell, P.J. Ioannou, Transient and asymptotic growth of two-dimensional perturbations in viscous compressible shear flow, *Physics of Fluids* 12 (2000) 3021–3028.
[25] A. Hanifi, P.J. Schmid, D.S. Henningson, Transient growth in compressible boundary layer flow, *Physics of Fluids* 8 (1996) 826–837.
[26] G. Ben-Dov, V. Levinski, J. Cohen, Optimal disturbances in swirling flows, *AIAA Journal* 42 (2001) 1841–1848.
[27] M.E. Goldstein, Unsteady vortical and entropic distortions of potential flows round arbitrary obstacles, *Journal of Fluid Mechanics* 89 (1978) 433–468.
[28] N. Peake, E.J. Kerschen, Influence of mean loading on noise generated by the interaction of gusts with a flat-plate cascade: upstream radiation, *Journal of Fluid Mechanics* 347 (1997) 315–346.
[29] T. Kato, *Perturbation Theory for Linear Operators*, Springer, Berlin, 1976.
[30] A. Pazy, *Semigroups of Linear Operators and Applications to Partial Differential Equations*, Springer, Berlin, 1983.
[31] M.R. Khorrami, A Chebyshev spectral collocation method using a staggered grid for the stability of cylindrical flows, *International Journal for Numerical Methods in Fluids* 12 (1991) 825–833.
[32] C.J. Heaton, N. Peake, Algebraic and exponential instability of inviscid swirling flow, *Journal of Fluid Mechanics*, 2006, submitted.
[33] A.J. Cooper, Effects of mean entropy on unsteady disturbance propagation in a slowly-varying duct with mean swirling flow, *Journal of Sound and Vibration* 291 (2006) 779–801.